Leaching behaviour of a crystallisation inhibitor in mortars

Kamat, Ameya; Lubelli, Barbara; Schlangen, Erik

DOI
10.1016/j.jobe.2023.107933

Publication date
2023

Document Version
Final published version

Published in
Journal of Building Engineering

Journal of Building Engineering 79 (2023) 107933

Contents lists available at ScienceDirect

Journal of Building Engineering

journal homepage: www.elsevier.com/locate/jobe

Leaching behaviour of a crystallisation inhibitor in mortars

Ameya Kamat [a,b,*], Barbara Lubelli [a], Erik Schlangen [b]

[a] Heritage and Architecture, Architecture and Built Environment, Delft University of Technology, the Netherlands
[b] Materials and Environment, Civil Engineering and Geosciences, Delft University of Technology, the Netherlands

ARTICLE INFO

Keywords:
Natural hydraulic lime mortar
Crystallisation inhibitor
Sodium ferrocyanide
Leaching
Diffusion
Advection
Sodium chloride
Salt damage

ABSTRACT

This paper investigates the leaching behaviour of sodium ferrocyanide, a known crystallisation inhibitor of sodium chloride, which is added to mortars for mitigation of salt decay. Leaching and depletion of the inhibitor is a practical performance related issue that might over time, make the inhibitor less effective against salt decay. In this research, the inhibitor was added to natural hydraulic lime (NHL) mortars during the mixing stage. Leaching of the inhibitor from the hardened mortar was assessed experimentally in laboratory. Both diffusion- and advection-driven transport mechanisms were considered. Diffusion experiments were carried out in a tank leaching test setup. Capillary absorption and drying cycles were used as a driving force to study advection-driven transport. Quantification of the leached species was carried out using various analytical techniques, including UV-VIS spectroscopy, ICP-OES and ion chromatography. The results from the tank leaching test show a high effective diffusion coefficient of ferrocyanide ions, in the same order of magnitude as sodium chloride transport. The advection test shows accumulation of the inhibitor at the evaporative surface and depletion of the inhibitor in the inner layers with successive wet-dry cycles. Based on these results it can be inferred that the degree of inhibitor leaching is significant and needs to be minimised to prolong the positive effect of the inhibitor on mortar durability. Potential solutions to reduce inhibitor leaching are discussed.

1. Introduction

Salt crystallisation in pores can result in significant damage to building materials, such as brick, natural stone and mortars. The damage is attributed to the development of crystallisation pressure as salt crystals grow against confined pore walls [1–3]. Soluble salts like sodium sulphate (Na_2SO_4) [4,5] and sodium chloride (NaCl) [6,7] are commonly found in buildings and responsible for salt crystallisation damage. NaCl, despite being much less damaging than sodium sulphate in accelerated crystallisation tests is found to cause severe decay in the field, in a wide range of environments [8]. Salt-spray, groundwater and de-icing salts are some of the common sources for NaCl accumulation in buildings [9]. Repeated crystallisation-deliquescence of NaCl crystals have shown to aggravate the damage [10,11]. Exposed parts of the buildings (e.g. plasters and renders) are particularly susceptible to salt induced weathering, due to repeated crystallisation-deliquescence cycles on account of a continuously changing environment (temperature and humidity changes) [12]. The damage manifests in the form of progressive material loss and is noticeably evident in the built cultural heritage. In fact, ancient mortars, which are mostly based on (hydrated) lime, are particularly vulnerable to salt crystallisation pressures, due to their low mechanical strength [13] and high potential to accumulate salts [14]. However, even in modern concrete, physical salt attack is of concern and cannot be neglected [15]. Current conservation techniques against salt damage, such as

* Corresponding author. Delft University of Technology, Faculty of Architecture, Julianalaan 134, Delft, 2628BL, Delft, the Netherlands.
E-mail address: a.a.kamat@tudelft.nl (A. Kamat).

https://doi.org/10.1016/j.jobe.2023.107933
Received 15 May 2023; Received in revised form 6 October 2023; Accepted 10 October 2023
Available online 11 October 2023

desalination, are costly and not always feasible [16]. Repair materials, such as stone-repair mortars and renovation plasters and renders, often have a limited durability and/or compatibility with the existing materials [17]. In the last decades, considerable research has been undertaken to seek alternative, durable solutions. The use of crystallisation inhibitors in porous building materials has shown promising results in numerous studies.

Crystallisation inhibitors are chemical compounds that modify salt crystallisation. Ionic compounds containing ferrocyanide ions ($Fe(CN)_6^{4-}$) such as sodium ferrocyanide (NaFeCN) or potassium ferrocyanide (KFeCN), are known to inhibit sodium chloride (NaCl) crystallisation by increasing supersaturation and thereby delaying the onset of crystal nucleation [18]. This favours mass transport of solutes over longer distances before precipitation [19]. Selwitz and Doehne were first to study the potential of alkali ferrocyanides as a treatment for salt damage mitigation in porous building materials [20]. The authors reported an increase in the amount of efflorescence and a decrease in damage in porous limestone contaminated with NaCl in presence of KFeCN, when compared to specimens contaminated with NaCl only. Alkali ferrocyanides are also shown to be habit modifiers, altering NaCl crystal from a regular cubic structure to a dendritic pattern [21]. Changes to the crystal habit are a result of a charge mismatch between $Fe(CN)_6^{4-}$ ion and the sodium chloride cluster blocking further crystal growth, by forming weak inter-crystal bridges [22]. This habit modification makes alkali ferrocyanides excellent anticaking agents for table salt, by preventing agglomeration of big crystals [23]. Studies in building materials also confirm NaFeCN's anticaking activity in increasing nucleation density and forming smaller NaCl crystals [24]. This could prevent pore clogging and reduce crystallisation pressure. Additionally, the dendritic crystal structure has shown to increase the surface area of salt crystals, thereby contributing to faster evaporation and salt transport to the surface [25]. Other studies performed on various porous substrates (stones, bricks, mortars and soil) have reported similar results i.e. increased salt (NaCl) transport out of the substrate (efflorescence), modification of the crystal habit and most importantly, minimal material damage in presence of $Fe(CN)_6^{4-}$ ions [21,26–29].

In recent years, hydrated lime mortars with mixed-in inhibitors have been tested with positive results [30]. A notable difference with the previous studies is the way the inhibitor is introduced to the porous substrate. In these studies, NaFeCN was added directly during the mortar preparation (mixing) stage. Accelerated salt weathering tests showed lower damage on specimens with the inhibitor compared to control specimens [31–33]. This was also evident in a case study, where hydrated lime plaster with mixed-in NaFeCN showed negligible material loss when applied on a salt-contaminated brick wall, after a period of 4 years [34]. Moreover, research has shown that the addition of inhibitor up to 1 % of binder weight to lime mortars (hydrated or hydraulic) does not affect the physical and chemical properties of mortar [35,36]. All these studies point towards NaFeCN/KFeCN as a suitable crystallisation inhibitor to be mixed in mortars in order to mitigate NaCl-induced decay.

In spite of all the mentioned advantages, one issue could limit the application of NaFeCN in mortar. Sodium ferrocyanide decahydrate, a commonly used source of $Fe(CN)_6^{4-}$ ions, has a high water solubility (17 g/100 mL at 25 °C) [37] and might leach out with time, losing its positive effect. Some preliminary observations from past research suggest that this inhibitor might leach out during wet-dry cycles [31] and accumulate at the outer surface due to capillary transport [34]. However, until now no systematic study is done to understand the inhibitor transport and its consequent leaching.

In porous materials, two mechanisms play an important role in transport of the inhibitor: Diffusion and advection. In fact, in all practical situations a competition of advection leading to accumulation (and crystallisation) of solute near the surface and simultaneous levelling of the concentration gradient due to diffusion dictates the transport mechanism [38]. Study of both mechanisms is equally relevant to understand the leaching behaviour. Studying the degree of leaching under both, diffusion and advection, will help in improving the durability of mortars with mixed-in NaFeCN.

This paper investigates transport and leaching of the NaFeCN inhibitor in mortar specimens made with natural hydraulic lime (NHL). In the first part, diffusive transport in mortar specimens containing the inhibitor is studied under controlled conditions using a standard test. The effective diffusion coefficient of $Fe(CN)_6^{4-}$ ions from mortar is measured and compared to effective diffusion coefficient of chloride ions from mortar specimens with similar properties. In the second part of the paper, advection driven inhibitor transport under realistic conditions is simulated experimentally. Capillary wetting and drying cycles are used as a driving force for advection. The changes to the spatial distribution of the inhibitor are monitored. The results from the two tests are discussed and solutions are proposed to minimise leaching.

2. Materials and methods

2.1. Test materials, specimen preparation and storage

Natural hydraulic lime (NHL) with a strength class of 3.5 was used as the binder. Standard river sand conforming to NEN-EN 196-1 [39] with a particle size distribution between 0.08 and 2 mm was used in mortar preparation. Laboratory grade reagent sodium ferrocyanide decahydrate (chemical formula: $Na_4Fe(CN)_6.10H_2O$) purchased from Acros organics was used as the crystallisation inhibitor. Laboratory grade sodium chloride (NaCl) was purchased from Sigma Aldrich.

Mortar was cast as cylindrical specimens (Φ = 30 mm and H = 50 mm) in smooth PVC cylindrical containers. Three types of cylindrical specimens were prepared: (1) Reference samples without any inhibitor [R]. (2) Specimens containing the inhibitor [I]. (3) Specimens containing sodium chloride [S]. All the specimens were cast with NHL and sand in a volumetric proportion (1:3). A water-binder (w/b) ratio of 1.19 was used for all mixes, based on the flow requirements of 165 mm [40] measured on the reference mix [R]. Mixing was carried according to the standards [40].

For specimens containing the inhibitor [I], sodium ferrocyanide decahydrate (abbreviated as NaFeCN), in the amount equivalent to 10 % by weight of the binder, was first dissolved in the water used for mixing (0.17 mol kg^{-1}) and then added to NHL and sand. This very high concentration of the inhibitor, much higher than that used in past research (1 %) [31], was necessary to stay within detection

limits of the used analysis techniques (Section 2.3.2).

For specimens containing salt [S], NaCl, in the amount of 0.17 mol kg^{-1} (corresponding to 1.17 % of the binder weight) was first dissolved in water and then added to NHL and sand during mixing. This way, [S] and [I] specimens contained the same concentration of Cl^- and $Fe(CN)_6^{4-}$ ions respectively, making possible to compare the leaching of these ions across different specimens.

An overview of specimen mix design is shown in Table 1.

All specimens were cured in the fog room at > 95 % RH and 20 °C. Specimens were kept sealed inside PVC cylindrical containers with a screw lid to avoid any leaching during the curing stage and cured for at least 28 days.

Additionally, binder paste (without sand) specimens corresponding to [R], [S] and [I] were prepared to measure fresh properties. For paste specimens, w/b = 1 was used. The specimens were tested immediately after mixing.

2.2. Materials characterisation

The aim of this section is to evaluate if different types of specimens [R], [I] and [S] used in the leaching tests are comparable to each other. Relevant properties that affect moisture and salt transport are studied in detail.

An overview of characterisation tests is shown in Table 2. Their open porosity, bulk density and pore size distribution were measured using mercury intrusion porosimetry (MIP) (Autopore IV by Micromeritics). The test was performed on samples ~1 cm^3, freeze dried after the curing period.

Water absorption via capillary suction was performed according to the NEN-EN 1925 standard [41]. The Capillary Moisture Content (CMC) and the time required for reaching CMC was obtained. At the end of the absorption test, the bottom side of the specimens was sealed with a paraffin film and the specimens were dried at 20 °C and 50 % RH. The specimens were weighed at defined time intervals, to obtain the drying curve.

The heat of hydration was measured on [R], [S] and [I] paste specimens. Measurements were carried out at a constant temperature of 20 °C for a period of 7 days, using calorimeter (Tam-AIR).

2.3. Leaching by diffusion

This test aims to study leaching of the inhibitor from mortar specimens under diffusion driven transport. The rate of leaching is obtained by estimating the effective diffusion coefficient of the inhibitor leached from mortar specimens [I] under controlled conditions. This is compared to the effective diffusion of chloride ions, as measured on mortar specimens [S], which are tested independently. In this way, rate of leaching of the inhibitor relative to the rate of leaching of salts (NaCl) is obtained from a similar type of mortar.

2.3.1. Test setup for study of leaching

The leaching test is based on ASTM C1308-21 standard [42]. The ASTM procedure was chosen as it enables to estimate the effective diffusion coefficient in a relatively short time (10 days).

The cylindrical mortar specimens (Section 2.1) were suspended in a plastic cylindrical tank using a fishing line as shown in Fig. 1 (a). A known volume of deionised water was added as the leachant (V_l). V_l was chosen such that the ratio of the surface area of the specimen (S) and the volume of the leachant (V_l) was 0.15 cm^{-1}. The leachate (leachant with dissolved species) was renewed using exactly the same volume (V_l) of deionised water, at the prescribed time intervals as per the standard. Prior to each renewal step, 20 mL of leachate was collected as an eluate analysed for relevant leached ions (section 2.4.3). The temperature and humidity in the lab were recorded and found to be around 25 °C and 55 % RH. The test was conducted in two series, as shown in Fig. 1(b). In the first series, one reference specimen [R] and 3 replicates of specimens containing the inhibitor [I] were tested for leaching of the inhibitor ($Fe(CN)_6^{4-}$ ions). In the second series, one reference specimen [R] and 3 replicates of specimens containing sodium chloride [S] were tested for the leaching of chloride ions. For the sake of simplicity, possible binding of chloride (or $Fe(CN)_6^{4-}$ ions) to mortar components was not taken into account.

The cold water extraction (CWE) test based on the work done by Plusquellec et al. [43] was used to estimate amount of inhibitor present in the mortar specimens. The test was conducted on:

- [I] and [S] specimens that were tested in the tank leaching test, to determine the amount of inhibitor (or chlorides) left within the specimens at the end of the test. The results were then used as an input to calculate the effective diffusion coefficient (Section 2.3.3).
- [I] and [S] specimens not used for the leaching test, to estimate the initial amount of inhibitor and chloride respectively and validate the findings from the tank leaching test.

The specimens were first dried in an oven at 40 °C until constant mass. The entire specimens were then crushed to a fine powder in a Retsch ball milling machine. An amount of demineralised water equal to the dry weight of the specimen was added to the finely ground

Table 1
Mix design of mortar and different types of specimens used.

Component	Reference [R]	Inhibitor [I]	Salt [S]
Binder: Sand [volume]	1:3	1:3	1:3
w/b	1.19	1.19	1.19
$Na_4Fe(CN)_6 10H_2O$ [mol kg^{-1}]	–	0.17	–
NaCl [mol kg^{-1}]	–	–	0.17

Table 2
Characterisation tests and type of specimens.

Material property	Test	Type of specimen	Specimen size	Number of Replicates
Pore size distribution Open porosity Bulk density	MIP	Mortar specimens [R], [I], [S]	1 cm^3	2
Heat of hydration	Isothermal calorimetry	Binder paste [R], [I], [S]	5 g	2
Water absorption and drying	Gravimetry	Mortar specimens [R], [I], [S]	Φ = 30 mm H = 50 mm	3

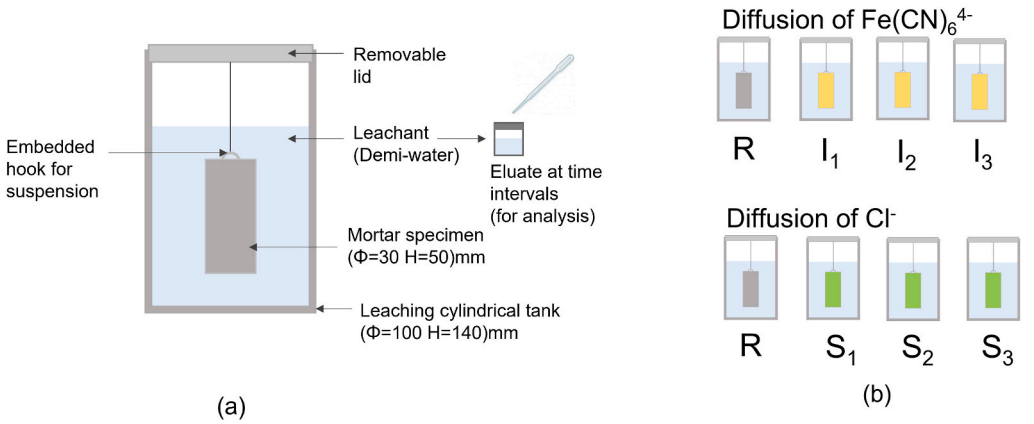

Fig. 1. (a) Experimental setup for leaching by diffusion (b) Series of specimens tested in the test.

powder. The mixture was stirred at 600 rpm for 5 min using a magnetic stirrer at room temperature. The free species were then allowed to dissolve for 24 h. Subsequently, a sample (5 mL) was passed through a qualitative medium speed filter and analysed for relevant species. Samples from [I] specimens were analysed using ICP-OES to quantify the present Fe ions. Samples from [S] specimens were analysed using ion-chromatography (IC), for measuring the amount of Cl ions (See section 2.3.2).

The initial amount of species ($Fe(CN)_6^{4-}$ or Cl^-) was calculated as per Equation (1) where: A_0 [mg] = absolute amount of species present at the start of the test; a_n [mg] = absolute amount of species leached at each n time interval. The absolute value a_n was obtained my multiplying the measured concentration [mg/L] with V_l [mL].

a_f [mg] = absolute amount of species left in the specimen at the end of the leaching test. The absolute value a_f was obtained my multiplying the measured concentration [mg/L] with the volume of water used in CWE [mL].

$$A_0 = \sum_{n=1}^{N} a_n + a_f \tag{1}$$

2.3.2. Eluate analysis: quantification of leached species

2.3.2.1. Ultraviolet–visible (UV-VIS) spectroscopy. A spectrophotometer (Shimadzu UV2600) was used to quantify the concentration of

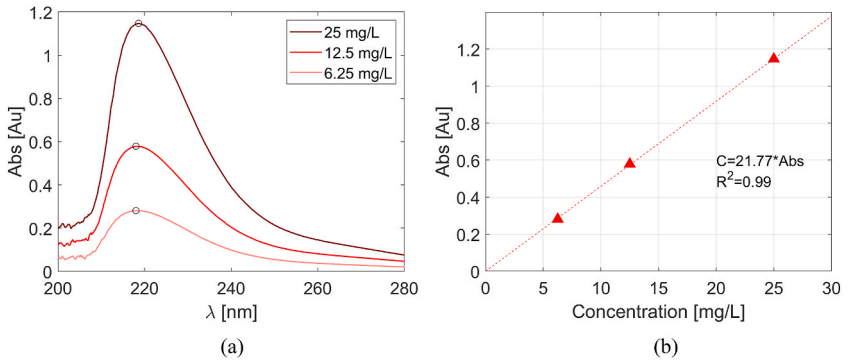

Fig. 2. UV-VIS calibration using solutions containing sodium ferrocyanide with known concentrations (a) Presence of $Fe(CN)_6^{4-}$ shows a strong peak at 218 nm (b) correlation between measured absorbance and concentration of sodium ferrocyanide obtained using linear regression.

NaFeCN in eluates. In the presence of $Fe(CN)_6^{4-}$ ions, a strong absorption peak is measured at a wavelength of 218 nm [18,44]. The concentration was measured as per Equation (2), following the Beer-Lambert's law [45].

$$Abs = \log_{10}\left(\frac{I_0}{I}\right) = k \bullet C \tag{2}$$

Where, (Abs) is the characteristic wavelength, C is the concentration of NaFeCN, k is the proportionality constant, and I_0 and I correspond to the incident and the transmitted light intensity respectively.

The optical path length of 1 cm was used for all the samples. The value of k was obtained by performing a linear regression with three freshly prepared standard solutions containing 25 mg/L, 12.5 mg/L and 6.25 mg/L of NaFeCN (Fig. 2(b)). Samples showing high absorbance (>1.5) were diluted such that the results remained within the linear calibration range.

2.3.2.2. Inductive coupled plasma optical emission spectroscopy (ICP). ICP was performed as a complimentary technique to cross validate the results obtained using UV-VIS. The eluates from [I] specimens were measured for Fe(II)/Fe(III) cations. 1 mL of the sample was diluted and acidified with 9 mL of 2 % (v/v) HNO_3 and analysed using optical emission spectrometer (PerkinElmer Optima 5300DV).

2.3.2.3. Ion chromatography (IC). IC was performed on eluates of the sampled leachate from [S] specimens to measure the chloride content. Dionex ICS 90 (by Thermo Fischer) ion chromatographs were used. The anions were separated using AS14A column where a solution of Na_2CO_3 and $NaHCO_3$ was used as an eluent.

2.3.3. Model for estimation of the effective diffusion coefficient

The amount of the leached species measured at each time step was used to estimate the effective diffusion coefficient (D_e) of the inhibitor and chloride ions from [I] and [S] specimens respectively, as per finite cylindrical model presented in the standard [46].

As a first step, at each time interval (n), the leached species (i.e., $Fe(CN)_6^{4-}$ or Cl^-) are expressed as cumulative fraction leached (CFL), which is a dimensionless quantity. The CFL at nth interval is calculated as per equation (3).

$$CFL_n = \sum_{n=1}^{N} \frac{a_n}{A_0} \tag{3}$$

The analytical solution is presented in Equation (4) [46],. The test setup and the analytical solution assume the same boundary conditions. A complete mathematical derivation using Fourier-Bessel series can be obtained from the works of Nestor and Pescatore [47,48]. The CFL obtained from Equation (3) is fitted to Equation (4) in order to obtain the effective diffusion coefficient D_e .

$$CFL = \left(1 - \frac{32}{\pi^2} S_p(t) S_c(t)\right) \tag{4}$$

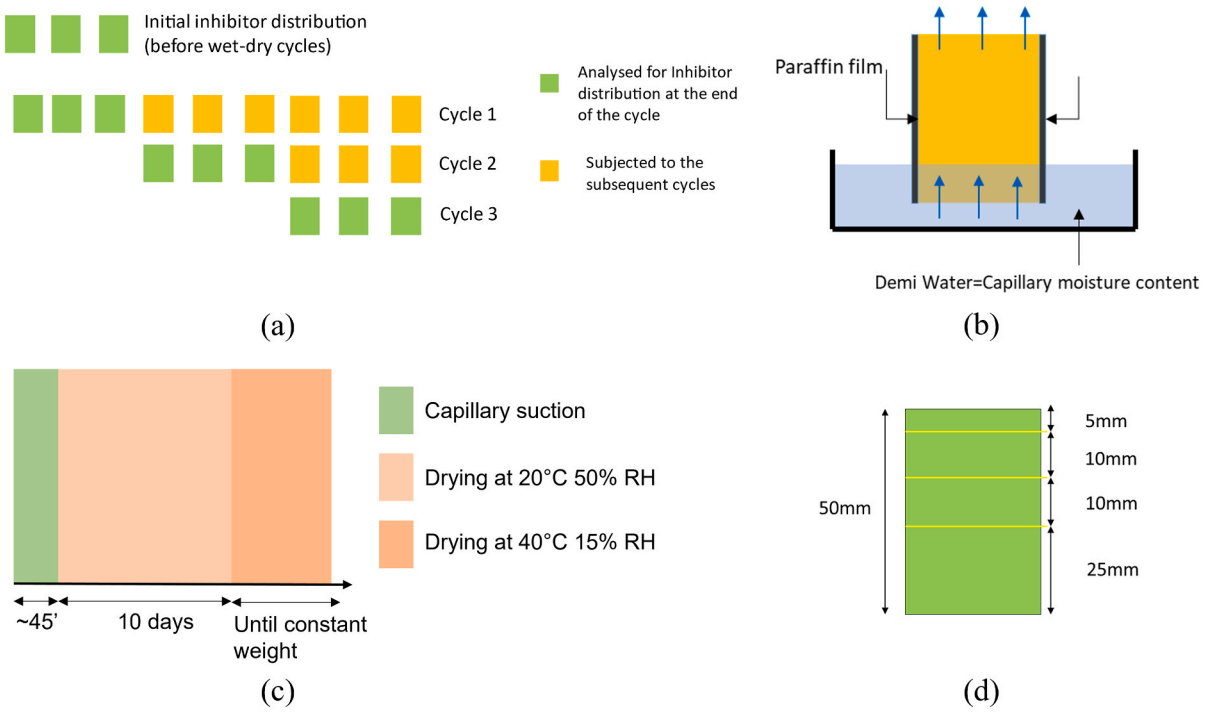

Fig. 3. (a) Overview of specimens used in each cycle (b) Schematic of capillary suction (c) Composition of the wet-dry cycle (d) schematic for inhibitor distribution.

With the series,

$$S_p(t) = \sum_{j=1}^{\infty} \frac{\exp\left(\left(-\frac{(2j-1)}{H}\pi\right)^2 D_e t\right)}{(2j-1)^2} \tag{5}$$

$$S_c(t) = \sum_{m=1}^{\infty} \frac{\exp\left(-\left[\frac{\beta_m}{R}\right]^2 D_e t\right)}{\beta_m^2} \tag{6}$$

Where, R is the radius of the specimen, H is the height of the specimen, t is the time. j represents the number of terms used in the series and m represents the series index that satisfy the zeroth order cylindrical Bessel function (β). A tolerance of 10^{-8} was used for the number of terms needed in the series for convergence during the iterative process.

2.4. Leaching by advection

The aim of the test is to monitor the advection-driven transport of inhibitor over the specimen height during repeated capillary absorption-drying cycles.

2.4.1. Test setup for study of advection

A scheme of the test setup is presented in Fig. 3. Twelve cylindrical specimens containing the inhibitor [I], prepared as described in Section 2.1, were used in this test. Before the start of the test, 3 specimens were analysed to assess the initial inhibitor distribution (see Section 2.4.2). The remaining 9 specimens were oven dried to a constant weight. Later, the sides of the specimens were sealed with a paraffin film to allow only for unidirectional flow. The specimens were subjected to 3 cycles of capillary suction via their bottom surface followed by drying via the opposite, evaporation surface. This procedure aims to replicate the moisture transport mechanism, which is common in the field, where plaster/renders are subjected to water supply (e.g., due to rising damp) from the wall on which they are applied and allowed to dry only through the exposed surface.

Each cycle consisted of three stages (Fig. 3 (c)). In the first stage, specimens were saturated with demineralised water via capillary suction (Fig. 3 (b)). The amount of water used for capillary absorption was equal to the maximum capillary moisture content value obtained from Table 3. After absorption was completed, the bottom of the specimens was sealed with a paraffin film. In the second stage, specimens were dried in a climate chamber at 20 °C and 50 % relative humidity. These conditions reflect common indoor field conditions and were used to facilitate liquid transport to the evaporative surface. In the third stage, at day 10, the specimens were moved to an oven at 40 °C/15 % RH. This procedure was defined in order to speed-up drying, without significantly affecting the transport of the inhibitor: after 10 days, the moisture content in the specimen is such that liquid transport does not play a significant role anymore and thus no further transport of the inhibitor can occur. At the end of each cycle, 3 specimens were used to analyse for the inhibitor distribution (Section 2.4.2), and the remaining specimens were subjected to the next cycle. During the test, the weight of the specimens was recorded regularly, and changes to the specimen surface were photographically recorded.

2.4.2. Distribution of the inhibitor

At the end of each wet-dry cycle, 3 specimens were brushed to remove any non-adhering efflorescence, which was collected and weighted separately. The specimens were then sliced over the depth (Fig. 3 (d)) with a dry saw and crushed to a fine powder. 500 mg of the powdered sample passed through 250 μm sieve was dissolved in 30 mL of demineralised water for 24 h. The concentration of inhibitor in each solution was analysed using UV-VIS (Section 2.3.2). Additionally, a small sample from the efflorescence developed on the top surface of the specimen was analysed using UV-VIS to quantify the amount of NaFeCN present in the efflorescent crust.

Environmental scanning electron microscope (ESEM) from FEI Quanta 650 FEG equipped with EDS (Noran EDS system) was used on a polished section of a mortar specimens subjected to one wet-dry cycle, in order to assess the inhibitor distribution in the outer 5 mm layer, by mapping of Fe, Na, N, Ca and Si. The specimen was epoxy impregnated to stabilise the mortar and sawed along the cross-section without using water. The cross-section was again impregnated with epoxy and polished using ethanol to prevent any dissolution of the NaFeCN crystals. The grinding and polishing procedure was followed as per past research [49]. The images were acquired at a voltage of 15 kV.

The crystal morphology of the NaFeCN crystals was studied on both a cross-section of the mortar and the efflorescence crust on the surface. Back-scattered electron (BSE) and secondary electron (SE) detectors were used. The sample for studying morphology was prepared by fracturing the mortar specimen along the height using a tensile splitting test.

Table 3
Overview of transport related properties.

Property	Reference [R]	Inhibitor [I]	Salt [S]
Porosity [%]	26.06 ± 0.92	24.43 ± 0.63	25.55 ± 0.02
Bulk Density [kg/m^3]	1963.5 ± 26.45	1997.3 ± 24.3	1973.5 ± 6.25
Capillary moisture content [% dry wt]	10.84 ± 0.15	9.7 ± 0.9	10.23 ± 0.35
Cumulative heat of hydration [J/g]	26.77 ± 3.25	25.61 ± 1.89	23.25 ± 5.25

3. Results

3.1. Materials characterisation

The pore size distribution of different types of specimens is presented in Fig. 4. It can be seen that the pore size distribution is similar for [R], [I] and [S] specimens. The heat of hydration (Fig. 5) also does not show formation of any anomalous hydrates due to the presence of inhibitor or salts. Other relevant microstructure properties (bulk density and open porosity) are shown in Table 3 and are comparable across different specimens.

The results of capillary absorption and drying behaviour are presented in Fig. 6. The rate of capillary absorption and the capillary moisture content across [R], [I] and [S] specimens are similar to each other.

The drying of [I] specimens (Fig. 6(b)) is significantly slower than the [R] and [S] specimens. A crust of the crystallised inhibitor is formed on the surface as shown in Fig. 11 (b) due to a high amount of the added inhibitor. This could have resulted in pore clogging and thereby slowing the drying process. Based on these results the drying cycle to be used in the study of advection (section 2.5.1) was defined.

3.2. Leaching by diffusion

The concentration of leached species measured at each renewal of water step is presented in Fig. 7. The trend obtained for [I] and [S] specimens, containing NaFeCN and NaCl respectively, is similar. The high concentration measured at the first time step (2 h) is related to surface washing rather than diffusion. For subsequent time steps, a diffusion controlled leaching process is observed.

No significant scatter is observed between results from replicates samples. The control samples as expected show absence of NaFeCN or NaCl. Therefore, the obtained results can be reliably used to estimate the effective diffusion coefficient, according to the procedure described in section 2.4.4.

A comparison of the effective diffusion coefficient (D_e) of $Fe(CN)_6^{4-}$ and Cl^- ions obtained by regression analysis is shown in Fig. 8. The model shows a good fit with the measured data and has a high coefficient of determination (R^2). It can be seen that the D_e for Cl^- transport is roughly twice that of $Fe(CN)_6^{4-}$ transport. This is logical, since a Cl^- ion has a smaller volume than a $Fe(CN)_6^{4-}$ ion. However, D_e of $Fe(CN)_6^{4-}$ is of the same order of magnitude of Cl^-, meaning the rate of leaching and the subsequent depletion of NaFeCN from the mortar is significant.

The remaining amount of $Fe(CN)_6^{4-}$ and Cl^- in the mortar specimens at the end of the leaching test is presented in Fig. 9, expressed as a percentage of the amount present at the start of the test. At the end of the leaching test, less than 20 % inhibitor was still present in the mortar, meaning more than 80 % inhibitor had leached out. In case of chloride, less than 10 % of the initial amount was left. The results of the CWE show slightly higher amount of remaining inhibitor, compared to the leaching test. A significant scatter is observed in CWE results; this can be due to the fact the CWE measurements were carried out on other specimens than those used in the leaching test or to the limited stirring (5 min) and dissolution time (24 h) used for in the CWE test, which might not be sufficient to fully dissolve NaFeCN, leading to underestimation of the initial inhibitor content. Taking the scatter into account, it can be concluded that the results obtained by CWE confirm and validate the results of the leaching test.

The eluates from [I] specimens were analysed by both UV-VIS for $Fe(CN)_6^{4-}$ and ICP for Fe ions. The results are presented in Fig. 10. The results obtained by these techniques are in good agreement. UV–Vis has the advantages of measuring the concentration of Fe $(CN)_6^{4-}$ ions (while ICP can only measure generic Fe ions). Furthermore, UV-VIS is a faster and an inexpensive method compared to ICP. Owing to these reasons, UV-VIS has been preferred to ICP in the following steps of this research.

3.3. Leaching by advection

The drying process and efflorescence development at each wet-dry cycle is presented in Fig. 11. An increase in the efflorescence, most probably (Na–FeCN crystallisation), is observed in time, indicating a progressive transport of the inhibitor to the surface. After

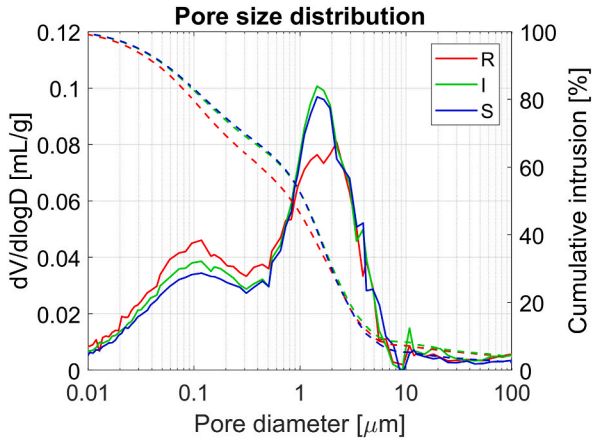

Fig. 4. Pore size distribution obtained using MIP.

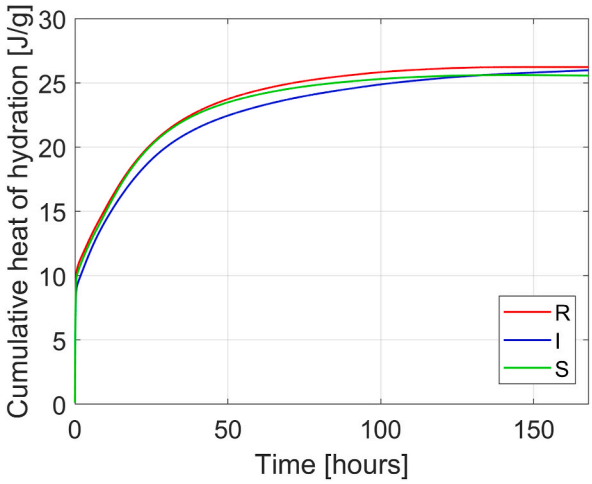

Fig. 5. Cumulative heat of hydration measured using isothermal calorimetry.

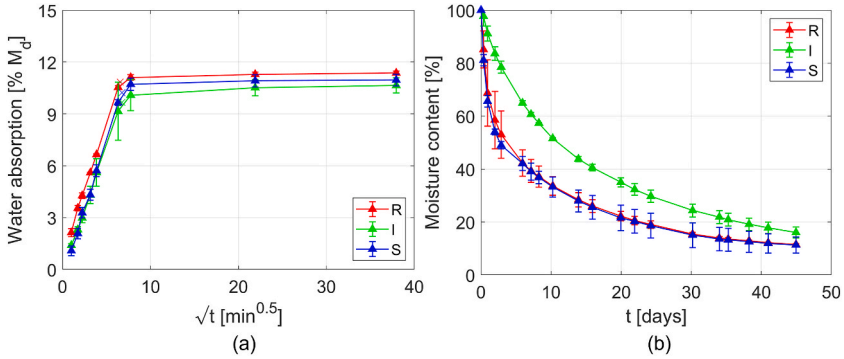

Fig. 6. (a) Water absorption due to capillary suction (b) drying behaviour.

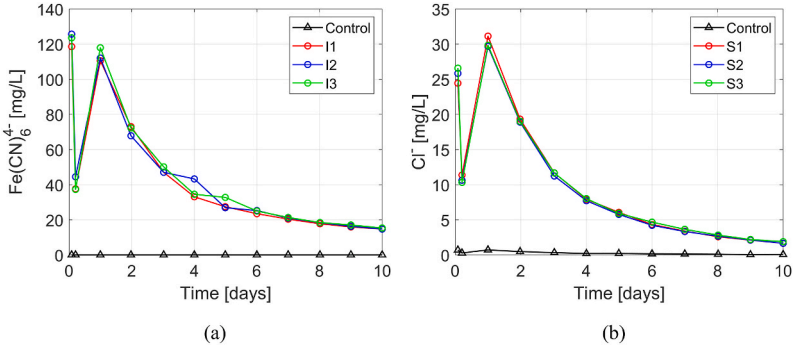

Fig. 7. Concentration measured at each renewal step (a) Sodium ferrocyanide using UV-VIS from [I] specimens (b) Chloride ions using Ion Chromatography from [S] specimens.

the end of the first cycle, there is a crust adhering to the top surface of the mortar specimens. After rewetting, the crust is seen to lift up. The effect of this is also partially evident in the drying process: the rate of drying is slow during the first cycle, when the well-adhering crust is delaying the evaporation. With subsequent cycles, when the curst was lifted up, the rate of drying increased.

The amount of inhibitor in the efflorescence and in the mortar specimens after each cycle was measured by UV-VIS. The non-adhering efflorescence was collected with a dry brush and weighed at the end of each cycle; at the end of the first cycle, no efflorescence could be collected, as they formed a crust very adherent to the surface.

The distribution of the inhibitor over the specimen height as assessed at the end of each cycle is shown in Fig. 12(a). At the start of the test, the inhibitor was homogenously distributed over the entire height of the sample. At the end of the first cycle, the inhibitor had

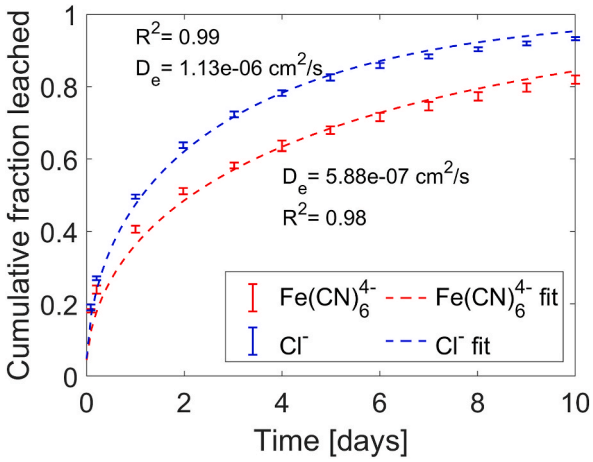

Fig. 8. Comparison of effective diffusion coefficient (D_e) between specimens containing the inhibitor ($Fe(CN)_6^{4-}$) and Cl^- obtained from regression analysis.

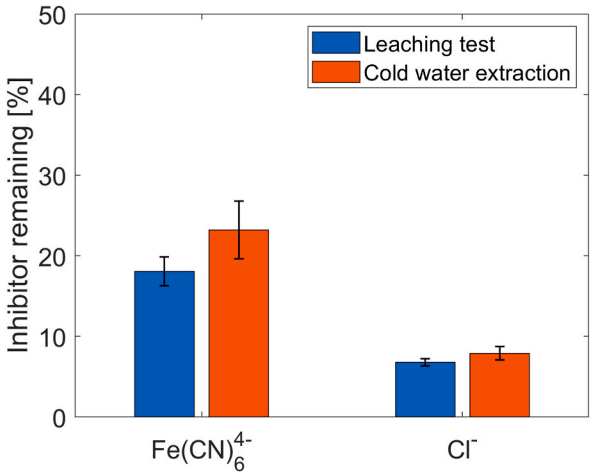

Fig. 9. Presence of inhibitor or chlorides present in the specimens at the end of the tank leaching test.

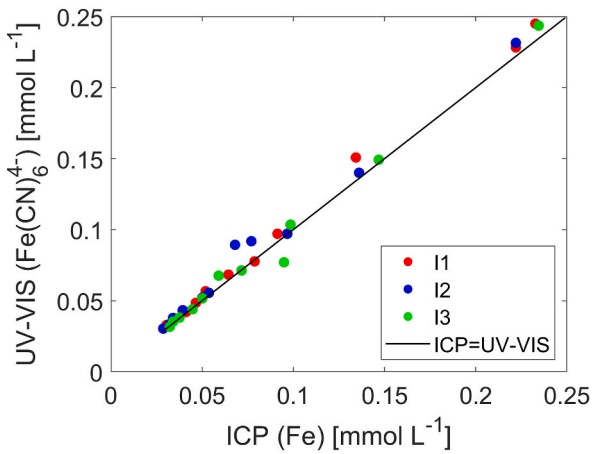

Fig. 10. Comparison of ICP and UV measurements for analysing inhibitor leaching.

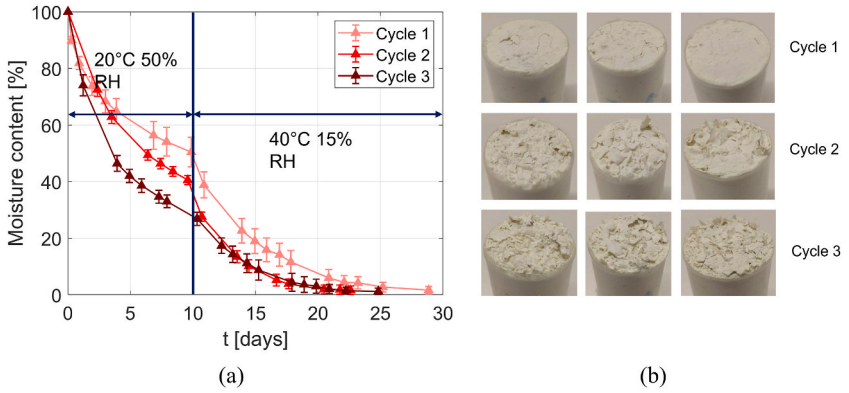

Fig. 11. (a) Moisture loss during the drying cycles (b) Visual inspection of the NaFeCN efflorescence/crust at the end of each cycle.

accumulated in the outer layer of the mortar specimen, at the evaporation surface. With successive cycling there was only a minor increase in the accumulation of the inhibitor in the top layer.

Fig. 12(b) shows the amount of efflorescence brushed from the surface at the end of the second and third cycle; it is evident that the amount of efflorescence increases with cycling. The composition of the efflorescence, analysed by UV-VIS, shows that these are mainly composed of NaFeCN (89.5 % by weight).

The SEM-EDS mapping of the specimen cross-section at the end of first cycle is presented in Fig. 13. Fig. 13(a) shows a lighter colour (indicating the presence of heavier elements) in the outer 200–400 μm: here a high concentration of Na, Fe and even N (low detection accuracy) is measured, confirming the massive presence of sodium ferrocyanide in this layer. The presence of NaFeCN is negligible beyond 400 μm from the evaporation surface. These results are in agreement with those of UV-VIS. Other components of mortar namely Ca and Si are, as expected, homogenously distributed in the mortar matrix. A thin layer of Ca is found at the very surface (Fig. 13(d)) possibly indicative of a binder-rich layer at the mortar surface.

The morphology of the crystallised inhibitor has been studied by BSE on a cross-section of the mortar and on parts of the detached efflorescence crust (Fig. 14). In the cross-section crystals of sodium ferrocyanide (NaFeCN) are visible in the mortar matrix. The efflorescence is entirely composed by crystals of NaFeCN, larger than those observed in the cross section.

4. Discussion and conclusions

In this study, the inhibitor leaching behaviour driven by diffusion and advection, has been experimentally investigated. The diffusion test, based on a combination of ASTM C1308-21 and cold water extraction, was able to reliably measure leaching of $Fe(CN)_6^{4-}$ ions from mortar under a concentration gradient. At the end of the diffusion test, more than 80 % of the inhibitor had leached out of the specimens, suggesting a strong ability of the inhibitor to transport under a concentration gradient. It should be mentioned that (1) The initial concentration of NaFeCN (10 % of binder weight) is higher than the concentration of the inhibitor necessary for obtaining the desired inhibition effect in actual mortars. This high concentration explains the high initial concentration gradient. (2) Replenishing leachant accelerates the flux of $Fe(CN)_6^{4-}$ ions by maintaining zero surface concentration. Despite the above mentioned points, the effective diffusion coefficient of $Fe(CN)_6^{4-}$ and Cl^- can be reliably compared, as the model considers the above parameters and measurements are done at the same experimental conditions. The effective diffusion coefficient of $Fe(CN)_6^{4-}$ (5.88×10^{-7} cm^2/s) is lower the Cl^- (11.3×10^{-7} cm^2/s) thus still in the same order of magnitude. This indicates that the inhibitor is expected to be transported only marginally slower compared to NaCl.

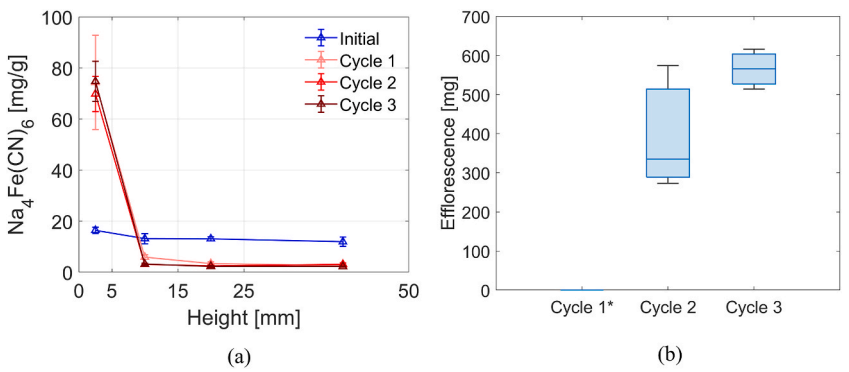

Fig. 12. (a) Inhibitor distribution over the height of the specimen (b) Weight of Na–FeCN efflorescence measured at the end of each cycle. * Cycle 1 had a tightly adherent efflorescent crust and was not weighed.

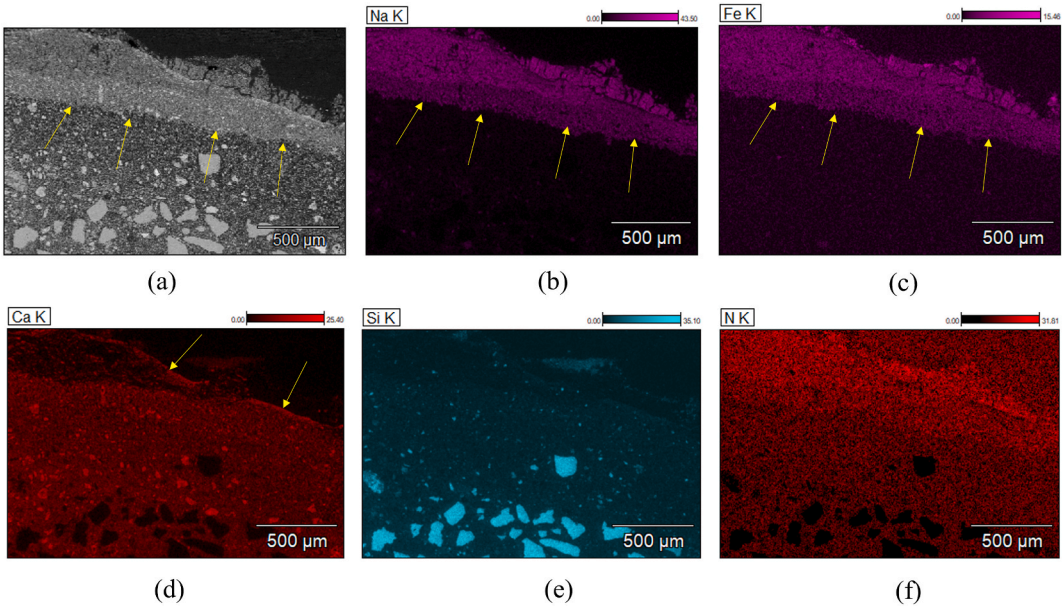

Fig. 13. SEM-EDS mapping of the outer 1.5 mm of the polished section of a mortar specimen after 1 wet-dry cycle. (a) Grey scaled image (b) sodium (Na) map (c) iron (Fe) map (d) calcium (Ca) map (e) silicon (Si) map and (f) Nitrogen (N) map. The yellow arrows in (a), (b) and (c) indicate accumulation of crystallised sodium ferrocyanide layer and (d) indicates presence of binder rich layer on the mortar surface. (For interpretation of the references to colour in this figure legend, the reader is referred to the Web version of this article.)

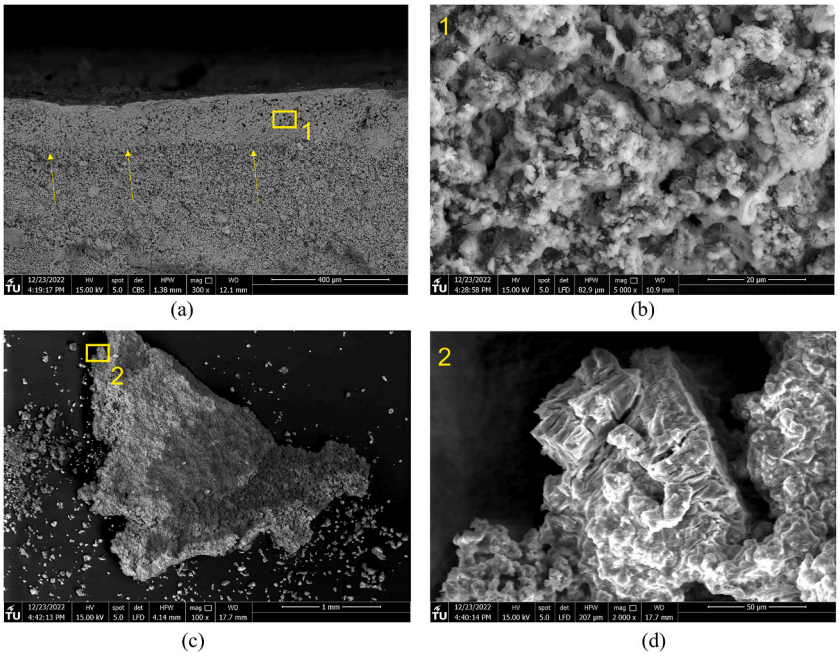

Fig. 14. SEM images for morphology (a) cross-section (b) magnified image of the cross-section (c) NaFeCN efflorescent crust (d) magnified image of the crust.

The advection test, consisting of capillary suction-drying cycles, confirmed that significant transport of the inhibitor occurs from depth to the evaporation surface. After one wetting-drying cycle, the inhibitor had accumulated at the surface of the mortar, in the form of a crust of efflorescence. In the outer layer of the mortar, inhibitor concentration increased 4 times to the initial concentration (at the start of the test). SEM-EDS observations confirmed that most of the inhibitor was localised within the first 400 μm from the outer surface. With successive cycling, an increase in the amount of efflorescence was observed at the specimen surface. UV-VIS spectrophotometry showed that 89.5 % by mass of the efflorescence was composed of sodium ferrocyanide (inhibitor).

The results from both diffusion and advection studies show high leaching rates of ferrocyanide in presence of water. This suggests

that this inhibitor, when mixed in the mortar, will be easily transported towards the surface and eventually leach out of the substrate or accumulate at the evaporative surface. This will lead to depletion of the inhibitor in the inner layers and its positive effect in mitigating salt decay may decline. It is therefore imperative to retard/slow down inhibitor leaching in order to prolong the durability of such mortars.

Different solutions can be envisaged to limit leaching of the inhibitor and ensure a longer service-life to the mortar. One way would be to reduce the mobility of $Fe(CN)_6^{4-}$ ions in the pore solution. This can be possibly done by encapsulating the inhibitor in (polymeric) capsules [50] instead of adding it directly to the mixing water. The polymeric capsule shells would constitute a barrier [51] to transport of the inhibitor into the pore solution. Possibly, capsule shells could be tuned to a smart release under external stimuli such as changes in pH [52,53] or presence of NaCl [54]. Research is on-going to assess these possibilities.

The methodology adopted in this research was successful in providing a quantitative analysis on the leaching of NaFeCN (crystallisation inhibitor) in mortar. This is the first instance that such a study has been undertaken on crystallisation inhibitors. Studying leaching of NaFeCN in other porous media e.g. natural stone and brine-contaminated soil could provide more relevant insights. Besides NaFeCN, other water soluble additives are vulnerable to leaching. A commonly used corrosion inhibitor in reinforced concrete, sodium nitrite is such an example [55]. The methodology can be further modified and extended to such additives. This can provide a better understanding in improving effectiveness of such additives across building materials.

CRediT author statement

Ameya Kamat: Conceptualization, Methodology, Formal analysis, Investigation, Writing-Original Draft, Barbara Lubelli: Conceptualization, Methodology, Writing-Review and Editing, Supervision, Project administration, Erik Schlangen: Conceptualization, Methodology, Writing-Review and Editing, Supervision, Project administration.

Declaration of competing interest

The authors declare that they have no known competing financial interests or personal relationships that could have appeared to influence the work reported in this paper.

Data availability

Data will be made available on request.

Acknowledgments

The research was financially supported by NWO (Dutch research council) under the project ‘Mortars with mixed-in inhibitors for mitigating salt damage-MORISAL’ (Grant no. 17636). The authors are grateful to Mr. Hans Dalderop from TU Eindhoven for assisting in ion chromatography and UV–Vis spectroscopy measurements. The authors thank Dr. Leo Pel for discussion and providing access to the lab facilities at TU Eindhoven. Additionally, the authors would like to thank Mr. Maiko van Leeuwen for technical assistance in preparation of the test setups, Mr. John van den Berg for performing ICP-OES measurements, Mr. Shan He for assisting with the ESEM study and Dr. Marija Nedeljković for proof reading and providing suggestions for making the manuscript more coherent.

References

[1] G.W. Scherer, Stress from crystallization of salt, Cem, Concr. Res 34 (2004) 1613–1624, https://doi.org/10.1016/j.cemconres.2003.12.034.
[2] R.J. Flatt, Salt damage in porous materials: how high supersaturations are generated, J. Cryst. Growth 242 (2002) 435–454, https://doi.org/10.1016/S0022-0248(02)01429-X.
[3] M. Steiger, Crystal growth in porous materials - I: the crystallization pressure of large crystals, J. Cryst. Growth 282 (2005) 455–469, https://doi.org/10.1016/j.jcrysgro.2005.05.007.
[4] R.J. Flatt, F. Caruso, A.M.A. Sanchez, G.W. Scherer, Chemo-mechanics of salt damage in stone, Nat. Commun. 5 (2014) 4823, https://doi.org/10.1038/ncomms5823.
[5] M. Schiro, E. Ruiz-Agudo, C. Rodriguez-Navarro, Damage mechanisms of porous materials due to in-pore salt crystallization, Phys. Rev. Lett. 109 (2012), 265503, https://doi.org/10.1103/PhysRevLett.109.265503.
[6] B. Lubelli, R.P.J. Van Hees, C.J.W.P. Groot, The role of sea salts in the occurrence of different damage mechanisms and decay patterns on brick masonry, Construct. Build. Mater. 18 (2004) 119–124, https://doi.org/10.1016/j.conbuildmat.2003.08.017.
[7] C. Gentilini, E. Franzoni, S. Bandini, L. Nobile, Effect of salt crystallisation on the shear behaviour of masonry walls: an experimental study, Construct. Build. Mater. 37 (2012) 181–189, https://doi.org/10.1016/j.conbuildmat.2012.07.086.
[8] B. Lubelli, V. Cnudde, T. Diaz-Goncalves, E. Franzoni, R.P.J. van Hees, I. Ioannou, B. Menendez, C. Nunes, H. Siedel, M. Stefanidou, V. Verges-Belmin, H. Viles, Towards a more effective and reliable salt crystallization test for porous building materials: state of the art, Mater. Struct. Constr 51 (2018), https://doi.org/10.1617/s11527-018-1180-5.
[9] A.E. Charola, C. Bläuer, Salts in masonry: an overview of the problem, Restor. Build. Monum 21 (2015) 119–135, https://doi.org/10.1515/rbm-2015-1005.
[10] B. Lubelli, R.P.J. Van Hees, H.P. Huinink, C.J.W.P. Groot, Irreversible dilation of NaCl contaminated lime-cement mortar due to crystallization cycles, Cement Concr. Res. 36 (2006) 678–687, https://doi.org/10.1016/j.cemconres.2005.10.008.
[11] J. Desarnaud, N. Shahidzadeh-Bonn, Salt crystal purification by deliquescence/crystallization cycling, EPL 95 (2011), https://doi.org/10.1209/0295-5075/95/48002.
[12] H. Derluyn, M. Griffa, D. Mannes, I. Jerjen, J. Dewanckele, A. Sheppard, D. Derome, V. Cnudde, E. Lehmann, I. Jerjen, J. Dewanckele, V. Cnudde, J. Carmeliet, Characterizing saline uptake and salt distributions in porous limestone with neutron radiography and X-ray micro-tomography, J. Build. Phys. (2013) 353–374, https://doi.org/10.1177/1744259112473947. Sagepub.Com/. 36.
[13] A. Moropoulou, K. Polikreti, A. Bakolas, P. Michailidis, Correlation of physicochemical and mechanical properties of historical mortars and classification by multivariate statistics, Cement Concr. Res. 33 (2003) 891–898, https://doi.org/10.1016/S0008-8846(02)01088-8.

[14] I. Papayianni, M. Stefanidou, V. Pachta, S. Konopisi, in: J.J. Hughes, J. Válek, C.J.W.P. Groot (Eds.), Content and Topography of Salts in Historic Mortars, Hist. Mortars, Springer International Publishing, Cham, 2019, pp. 119–126, https://doi.org/10.1007/978-3-319-91606-4_9.

[15] H. Haynes, R. O'Neill, M. Neff, P. Kumar Mehta, Salt weathering of concrete by sodium carbonate and sodium chloride, ACI Mater. J. 107 (2010) 258–266, https://doi.org/10.14359/51663754.

[16] V. Verges-Belmin, H. Siedel, Desalination of Masonries and Monumental Sculptures by Poulticing: a Review/Entsalzen von Mauerwerk und Steinfiguren mit Hilfe von Kompressen: ein Überblick, Restor. Build. Monum 11 (2005) 391–408, https://doi.org/10.1515/rbm-2005-6000.

[17] C. Groot, R. van Hees, T. Wijffels, Selection of plasters and renders for salt laden masonry substrates, Construct. Build. Mater. 23 (2009) 1743–1750, https://doi.org/10.1016/j.conbuildmat.2008.09.013.

[18] A. Glasner, M. Zidon, The crystallization of NaCl in the presence of [Fe(CN)6]4- ions, J. Cryst. Growth 21 (1974) 294–304, https://doi.org/10.1016/0022-0248(74)90018-9.

[19] R.D. Cody, Organo-crystalline interactions in evaporite systems; the effects of crystallization inhibition, J. Sediment. Res. 61 (1991) 704–718, https://doi.org/10.1306/D42677B7-2B26-11D7-8648000102C1865D.

[20] C. Selwitz, E. Doehne, The evaluation of crystallization modifiers for controlling salt damage to limestone, J. Cult. Herit. 3 (2002) 205–216, https://doi.org/10.1016/S1296-2074(02)01182-2.

[21] C. Rodriguez-Navarro, L. Linares-Fernandez, E. Doehne, E. Sebastian, Effects of ferrocyanide ions on NaCl crystallization in porous stone, J. Cryst. Growth 243 (2002) 503–516, https://doi.org/10.1016/S0022-0248(02)01499-9.

[22] A.A.C. Bode, V. Vonk, F.J. Van Den Bruele, D.J. Kok, A.M. Kerkenaar, M.F. Mantilla, S. Jiang, J.A.M. Meijer, W.J.P. Van Enckevort, E. Vlieg, Anticaking activity of ferrocyanide on sodium chloride explained by charge mismatch, Cryst. Growth Des. 12 (2012) 1919–1924, https://doi.org/10.1021/cg201661y.

[23] S.J. Dorazio, C. Brückner, Why is there cyanide in my table salt? Structural chemistry of the anticaking effect of yellow prussiate of soda (Na4[Fe(CN)6]·10H2O), J. Chem. Educ. 92 (2015) 1121–1124, https://doi.org/10.1021/ED500776B/SUPPL_FILE/ED500776B_SI_001.PDF.

[24] S. Granneman, Mitigating Salt Damage in Lime-Based Mortars by Built-In Crystallization Modifiers, Delft University Press, 2019, https://doi.org/10.4233/uuid:024d9d2e-cfbd-4753-b7cf-587799110824.

[25] S. Gupta, K. Terheiden, L. Pel, A. Sawdy, Influence of ferrocyanide inhibitors on the transport and crystallization processes of sodium chloride in porous building materials, Cryst. Growth Des. 12 (2012) 3888–3898, https://doi.org/10.1021/cg3002288.

[26] B. Lubelli, R.P.J. van Hees, Effectiveness of crystallization inhibitors in preventing salt damage in building materials, J. Cult. Herit. 8 (2007) 223–234, https://doi.org/10.1016/j.culher.2007.06.001.

[27] T. Rivas, E. Alvarez, M.J. Mosquera, L. Alejano, J. Taboada, Crystallization modifiers applied in granite desalination: the role of the stone pore structure, Construct. Build. Mater. 24 (2010) 766–776, https://doi.org/10.1016/j.conbuildmat.2009.10.031.

[28] K.L. Platt, D.M. Di Toro, R.F. Carbonaro, N.A. Bugher, T.F. Parkerton, L.J. Eastcott, P.T. Imhoff, Ferrocyanide enhanced evaporative flux to remediate soils contaminated with produced water brine, J. Hazard Mater. 442 (2023), 130028, https://doi.org/10.1016/J.JHAZMAT.2022.130028.

[29] S. Gupta, H.P. Huinink, L. Pel, K. Kopinga, How ferrocyanide influences NaCl crystallization under different humidity conditions, Cryst. Growth Des. 14 (2014) 1591–1599, https://doi.org/10.1021/cg4015459.

[30] B. Lubelli, T.G. Nijland, R.P.J. Van Hees, A. Hacquebord, Effect of mixed in crystallization inhibitor on resistance of lime-cement mortar against NaCl crystallization, Construct. Build. Mater. 24 (2010) 2466–2472, https://doi.org/10.1016/j.conbuildmat.2010.06.010.

[31] S.J.C. Granneman, B. Lubelli, R.P.J. van Hees, Effect of mixed in crystallization modifiers on the resistance of lime mortar against NaCl and Na2SO4 crystallization, Construct. Build. Mater. 194 (2019) 62–70, https://doi.org/10.1016/j.conbuildmat.2018.11.006.

[32] J. Feijoo, D. Ergenç, R. Fort, M.Á. de Buergo, Addition of ferrocyanide-based compounds to repairing joint lime mortars as a protective method for porous building materials against sodium chloride damage, Mater. Struct. 54 (2021) 14, https://doi.org/10.1617/s11527-020-01596-4.

[33] D. Ergenç, J. Feijoo, R. Fort, M. Alvarez de Buergo, Effects of potassium ferrocyanide used for desalination on lime composite performances in different curing regimes, Construct. Build. Mater. 259 (2020), 120409, https://doi.org/10.1016/j.conbuildmat.2020.120409.

[34] B. Lubelli, E. des Bouvrie, T.G. Nijland, A. Kamat, Plasters with mixed-in crystallization inhibitors: results of a 4-year monitoring of on-site application, J. Cult. Herit. 59 (2023) 10–22, https://doi.org/10.1016/j.culher.2022.10.016.

[35] S.J.C. Granneman, B. Lubelli, R.P.J. Van Hees, Characterization of lime mortar additivated with crystallization modifiers, Int. J. Architect. Herit. 12 (2018) 849–858, https://doi.org/10.1080/15583058.2017.1422570.

[36] A. Kamat, B. Lubelli, E. Schlangen, Effect of a mixed-in crystallization inhibitor on the properties of hydraulic mortars, AIMS Mater. Sci 9 (2022) 628–641, https://doi.org/10.3934/matersci.2022038.

[37] J.A.N. Friend, J.E. Townley, R.H. Vallance, CCCIII.—the solubility of sodium ferrocyanide in water between 0° and 104°, J. Chem. Soc. (1929) 2326–2330, https://doi.org/10.1039/JR9290002326.

[38] H.P. Huinink, L. Pel, M.A.J. Michels, How ions distribute in a drying porous medium: a simple model, Phys. Fluids 14 (2002) 1389–1395, https://doi.org/10.1063/1.1451081.

[39] Nen-En 196-1, Methods of Testing Cement - Part 1, Determination of strength, 2015.

[40] Nen-En 459-2, Building Lime-Part 2: Test Methods, 2008.

[41] Nen-En-1925, Natural Stone Test Methods- Determination of Water Absorption Coefficient by Capillarity, 1999.

[42] Astm C1308-21, Standard test method for accelerated leach test for measuring contaminant releases from solidified waste. https://doi.org/10.1520/C1308-21.2, 2021.

[43] G. Plusquellec, M.R. Geiker, J. Lindgård, J. Duchesne, B. Fournier, K. De Weerdt, Determination of the pH and the free alkali metal content in the pore solution of concrete: review and experimental comparison, Cement Concr. Res. 96 (2017) 13–26, https://doi.org/10.1016/j.cemconres.2017.03.002.

[44] M. Shirom, G. Stein, The absorption spectrum of the ferrocyanide ion in aqueous solution, Isr. J. Chem. 7 (1969) 405–412, https://doi.org/10.1002/ijch.196900051.

[45] D.F. Swinehart, The beer-lambert law, J. Chem. Educ. 39 (1962) 333, https://doi.org/10.1021/ed039p333.

[46] Astmc1308-08, Astm C1308-95, Standard test method for accelerated leach test for diffusive releases from solidified waste and a computer program to model diffusive, Fractional Leaching from Cylindrical Waste Forms (2001), https://doi.org/10.1520/C1308-08.2.

[47] C.W.J. Nestor, Diffusion from Solid Cylinders, 1980, https://doi.org/10.2172/5780257. Oak Ridge, TN (United States).

[48] C. Pescatore, Improved expressions for modeling diffusive, fractional cumulative leaching from finite-size waste forms, Waste Manag. 10 (1990) 155–159, https://doi.org/10.1016/0956-053X(90)90120-A.

[49] C. Nunes, A. Maria Aguilar Sanchez, S. Godts, D. Gulotta, I. Ioannou, B. Lubelli, B. Menendez, N. Shahidzadeh, Z. Slížková, M. Theodoridou, Experimental research on salt contamination procedures and methods for assessment of the salt distribution, Construct. Build. Mater. 298 (2021), 123862, https://doi.org/10.1016/j.conbuildmat.2021.123862.

[50] A.P. Esser-Kahn, S.A. Odom, N.R. Sottos, S.R. White, J.S. Moore, Triggered release from polymer capsules, Macromolecules 44 (2011) 5539–5553, https://doi.org/10.1021/ma201014n.

[51] J. Li, D.J. Mooney, Designing hydrogels for controlled drug delivery, Nat. Rev. Mater. 1 (2016) 1–18, https://doi.org/10.1038/natrevmats.2016.71.

[52] A. Kamat, D. Palin, B. Lubelli, E. Schlangen, Tunable chitosan-alginate capsules for a controlled release of crystallisation inhibitors in mortars, MATEC Web Conf 378 (2023), 02011, https://doi.org/10.1051/matecconf/202337802011.

[53] J. Wang, A. Mignon, G. Trenson, S. Van Vlierberghe, N. Boon, N. De Belie, A chitosan based pH-responsive hydrogel for encapsulation of bacteria for self-sealing concrete, Cem. Concr. Compos. 93 (2018) 309–322, https://doi.org/10.1016/J.CEMCONCOMP.2018.08.007.

[54] W. Xiong, J. Tang, G. Zhu, N. Han, E. Schlangen, B. Dong, X. Wang, F. Xing, A novel capsule-based self-recovery system with a chloride ion trigger, Sci. Rep. 5 (2015) 1–6, https://doi.org/10.1038/srep10866.

[55] J. Ress, U. Martin, J. Bosch, D.M. Bastidas, pH-triggered release of NaNO2 corrosion inhibitors from novel colophony microcapsules in simulated concrete pore solution, ACS Appl. Mater. Interfaces 12 (2020) 46686–46700, https://doi.org/10.1021/acsami.0c13497.